Available online at www.sciencedirect.com

ScienceDirect

journal homepage: www.elsevier.com/locate/he

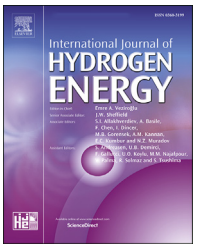

Properties of $BaYO_3$ perovskite and hydrogen storage properties of $BaYO_3H_x$

Aysenur Gencer [a,b,*], *Gokhan Surucu* [a,c,d]

[a] *Department of Physics, Middle East Technical University, Turkey*
[b] *Department of Physics, Karamanoglu Mehmetbey University, Turkey*
[c] *Department of Electric and Energy, Ahi Evran University, Turkey*
[d] *Photonics Application and Research Center, Gazi University, Turkey*

HIGHLIGHTS

- $BaYO_3$ perovskite has been investigated using Density Functional Theory (DFT).
- Hydrogen bonding to $BaYO_3$ perovskite has been performed and $BaYO_3H_3$ and $BaYO_3H_9$ have been obtained.
- The gravimetric hydrogen storage capacity is found to be 1.09 wt% for $BaYO_3H_3$

ARTICLE INFO

Article history:
Received 5 November 2018
Received in revised form
10 June 2019
Accepted 27 June 2019
Available online 20 July 2019

Keywords:
Hydrogen storage
Perovskite
Density functional theory
Electronic properties

ABSTRACT

In this study, Density Functional Theory (DFT) calculations have been performed for $BaYO_3$ perovskite with the generalized gradient approximation (GGA) as implemented in Vienna Ab-initio Simulation Package (VASP). The structural optimization of $BaYO_3$ perovskite have been studied for the five possible phases: cubic, tetragonal, hexagonal, orthorhombic and rhombohedral to determine the most stable phase of $BaYO_3$ perovskite. It has been found that the cubic phase is the most stable one and electronic and mechanical properties of this phase have been investigated. Moreover, the elastic anisotropy has been visualized in detail by plotting the directional dependence of compressibility, Poisson ratio, Young's and Shear moduli for cubic phase. Then, hydrogen bonding to $BaYO_3$ perovskite has been conducted and hydrogen storage properties of $BaYO_3H_x$ ($x = 3$ and 9) such as: formation energy, cohesive energy and gravimetric hydrogen storage capacity have been analyzed. Having no study about $BaYO_3$ perovskite and hydrogen bonding in the literature makes this study the first considerations of $BaYO_3$ perovskite. Hence, this work could enlighten the possible future studies.

Introduction

Hydrogen is the most abundant element in the Earth and its energy density is three times higher than the oil [1]. Hydrogen is a gas at ambient conditions therefore it can be stored in high pressure tanks which cause safety problems [2,3]. Liquid hydrogen storage can only be ensured at cryogenic temperatures and the energy is needed to liquefy the hydrogen [2,3].

* *Corresponding author*. Department of Physics, Middle East Technical University, Turkey.
E-mail address: agencer@kmu.edu.tr (A. Gencer).

https://doi.org/10.1016/j.ijhydene.2019.06.198
0360-3199/

Also, boiling off hydrogen is another issue for liquid hydrogen storage. Hydrogen could be physisorbed or chemisorbed for solid state hydrogen storage [2]. Physisorption of hydrogen needs low temperatures in order to have high hydrogen sorption because of the low Van der Waals force between material and hydrogen [4]. In contradiction to physisorption, there are chemical bonds for the chemisorption of hydrogen which requires high temperatures to release the hydrogen [5]. The hydrogen should be stored and released at ambient conditions, the material should have good kinetics and reversible storage of hydrogen for several times in order to get an efficient storage material [6]. Both gas, liquid and solid state hydrogen storage methods have some advantages and disadvantages. However, solid state hydrogen storage could be a long term solution.

Solid state hydrogen storage studies are mainly focused on carbon materials, metal hydrides and complex hydrides [7–15]. Carbon materials store hydrogen via physisorption of hydrogen and large pore size is necessary for high hydrogen adsorption. Despite having low pore size, the carbon nanotubes have high hydrogen storage capacities [15]. For the metal hydrides, MgH_2 is studied extensively in the literature that has high gravimetric hydrogen storage capacity with low hydrogen desorption kinetics [16–19]. Another promising material group for hydrogen storage is the Ni-based hydrides that are stable and have high kinetics [20–22]. Complex hydrides are generally composed of group 1A, group 2A and group 3A elements and the most studied complex hydrides are alanates, imides, borohydrides [3]. The disadvantage of complex hydrides is the non-reversible hydrogen storage. To overcome this issue, the catalyst has been added to the complex hydrides systems [23]. In addition, perovskite type hydrides have been studied for the solid state hydrogen storage both theoretically and experimentally [24–28]. Perovskite type hydrides are generally composed of group 1A and group 2A elements and hydrogen. Therefore, perovskite type hydrides have high gravimetric hydrogen storage capacity. As an example, $NaMgH_3$ perovskite type hydride has approximately 6 wt% gravimetric hydrogen storage capacity [29]. Also, addition of dopants could improve the hydrogen release from perovskite type hydrides. Li et al. [30]. Studied theoretically the effect of Li, Na, Rb and Cs dopants to $K_{1-x}M_xMgH_3$ where M = Li, Na, Rb and Cs and found that for hydrogen release, Li is the most effective dopant. Also, Wang et al. [31] reported the experimental study on the improvement of the dehydriding properties for $NaMgH_3$ with K_2TiF_6 dopant.

Perovskite materials are ceramic and they are hard materials therefore they could be a material candidate for efficient solid state hydrogen storage. But there is no study for perovskite materials in the literature except a recent study that present the hydrogen storage properties of $MgTiO_3H_x$ and $CaTiO_3H_x$ compounds [32]. The main motivation for this study comes from the potential applications for perovskite materials for the solid state hydrogen storage method. For this purpose, $BaYO_3$ perovskite has been chosen to investigate its hydrogen storage properties.

In this study, $BaYO_3$ perovskite has been investigated using Density Functional Theory (DFT) and then hydrogen bonding to $BaYO_3$ perovskite has been performed and the results have been analyzed. The calculation details and the structural optimizations will be detailed in Section Calculation details and structural optimizations. The electronic properties including band structure, corresponding

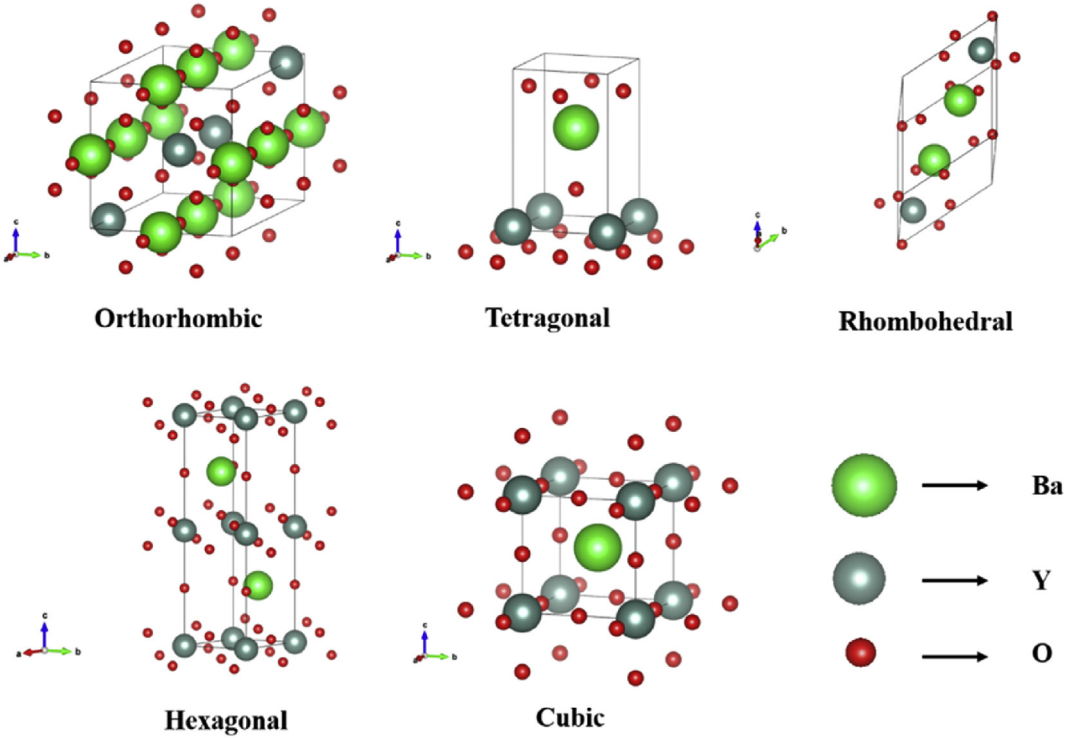

Fig. 1 – Crystal structure for $BaYO_3$ perovskite.

Table 1 – Lattice constants (lattice vectors: a, b, c in Å and the angles between the vectors: α, β, γ) and formation energies (ΔE_f in eV/atom).

	a	b	c	α	β	γ	ΔE_f
Orthorhombic (Pnma)	9.791	6.363	6.368	90.00	90.00	90.00	−1.10
Tetragonal (P4mm)	3.884	3.884	6.362	90.00	90.00	90.00	−2.26
Rhombohedral (R-3c)	6.608	6.608	6.608	55.49	55.49	55.49	−1.65
Hexagonal ($P6_3/mmc$)	3.935	–	14.152	90.00	90.00	120.00	−1.35
Cubic (Pm-3m)	4.428	–	–	90.00	90.00	90.00	−2.67

density of states, charge density and Bader partial charge analysis will be presented in section Electronic properties. Then, section Mechanical properties contains the calculation results for the mechanical properties. The hydrogen bonding studies and their results will be presented in section Hydrogen bonding studies. Finally, a brief summary will be given in Section Conclusion.

Calculation details and structural optimizations

All calculations have been performed by the self-consistent density functional theory (DFT) with a plane-wave pseudopotential approach implemented in the Vienna Ab initio Simulation Package (VASP) [33,34].

The pseudopotentials are employed according to Perdew-Burke-Ernzerhof (PBE) parametrization [35]. The generalized gradient approximation (GGA) is chosen for exchange correlation term for the electron-electron interaction. The projector augmented wave (PAW) method [36,37] is implemented for the electron-ion interaction. The cut off energy is chosen as 1000 eV. The k-point sampling has been done with a gamma centered [38] or Monkhorst-Pack scheme [39] according to the crystal structure. The structural optimizations have been performed for each structure and the k-points are chosen gamma centered scheme 10x10 × 8 for tetragonal phase (P4mm), 15 × 15 × 15 for cubic phase (Pm-3m), 12 × 12 × 3 for hexagonal phase ($P6_3/mmc$) and Monkhorst-Pack scheme 6x8x8 for orthorhombic phase (Pnma), 14 × 14 × 14 for rhombohedral phase (R-3c). To obtain well optimized structures, stresses and Hellman-Feynman forces are minimized using the conjugate gradient algorithm with the force convergence less than 10^{-9} eV $Å^{-1}$. For the iterative solution of the Khon-Sham equations, the energy tolerance is chosen 10^{-10} eV per unit cell. Ba, Y, and O valence electron configurations are considered as $5s^25p^66s^2$, $4s^24p^64d^15s^2$, and $2s^22p^4$, respectively. For the mechanical properties, elastic constants have been calculated using stress-strain method [33,34]. Bader partial charge calculation has been performed using VASP and analysis of the results have been done using the algorithm developed by Henkelman group [39] that is based on Bader's suggestion [40].

Fig. 1 shows the crystal structure for $BaYO_3$ perovskite that could crystalize in the five possible crystal structures: cubic (Pm-3m), tetragonal (P4mm), hexagonal ($P6_3/mmc$), orthorhombic (Pnma) and rhombohedral (R-3c) [41].

These structures have been studied in order to determine the most stable structure. Table 1 lists the optimized lattice parameters. In the literature, there is no experimental nor theoretical study in order to compare the calculated results as authors know up to date. Also, the formation energies have been calculated using Equation (1) and given in Table 1. If the formation energy is negative, this means that this structure could be synthesizable and energetically stable. For $BaYO_3$ perovskite, all the possible crystal structures are stable and synthesizable. Also, the cubic phase is the most stable phase because of having the lowest formation energy.

$$\Delta E_f = E_t(BaScO_3) - [E(Ba) + E(Sc) + 3 * E(O)] \quad (1)$$

After the structural optimizations, energy-volume and enthalpy-pressure graphs have been plotted in order to determine the most stable phase and phase transitions. Fig. 2 and Fig. 3 show formation energy as a function of volume and enthalpy as a function of pressure plots for $BaYO_3$ perovskite. As

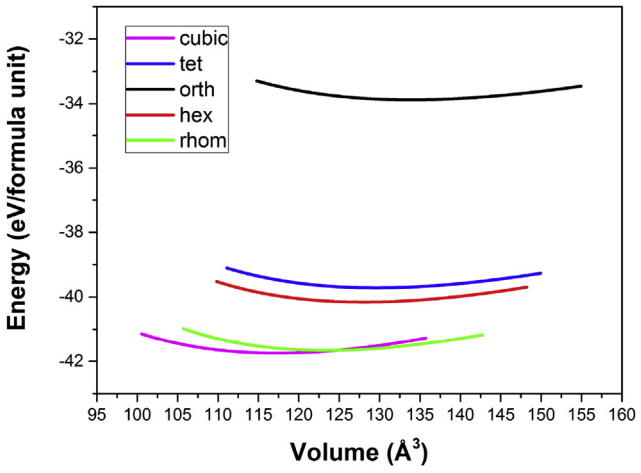

Fig. 2 – Energy-volume graph for $BaYO_3$ perovskite.

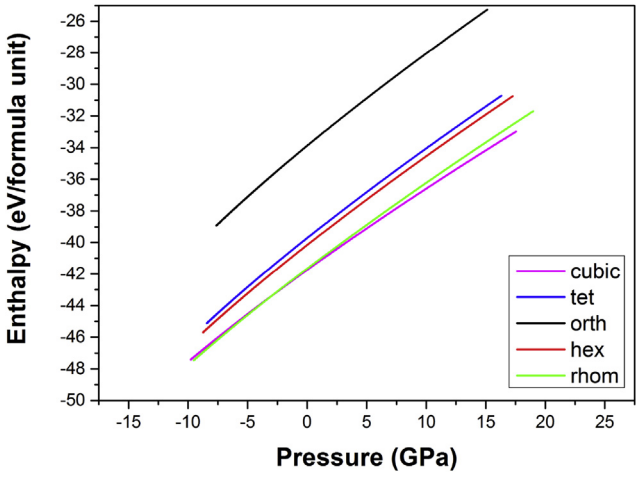

Fig. 3 – Enthalpy-pressure graph for $BaYO_3$ perovskite.

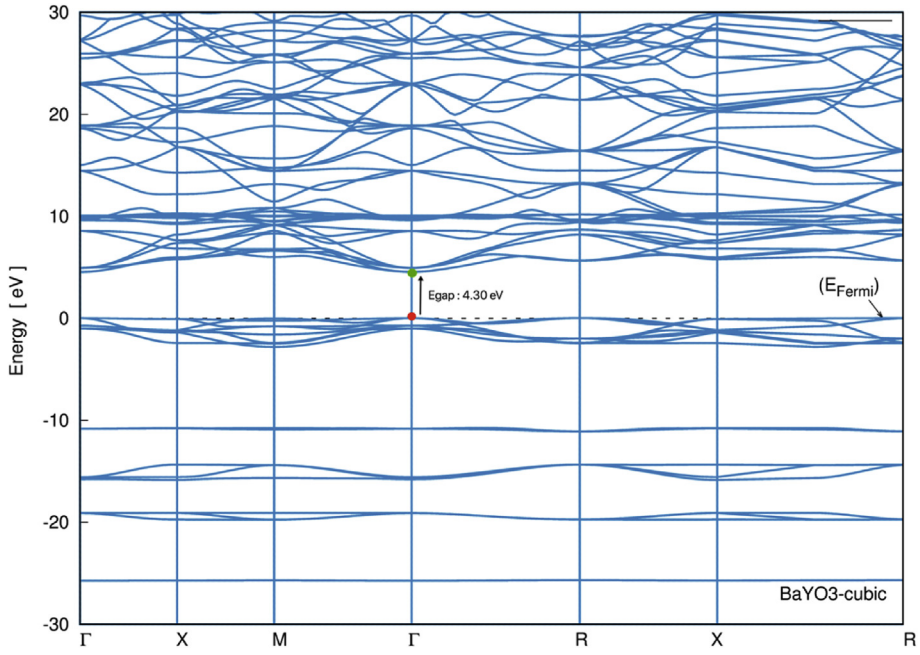

Fig. 4 – Band structure for $BaYO_3$ cubic phase.

can be seen from the figures, the cubic phase is the most stable phase for $BaYO_3$ at positive pressures which is consisted with the formation energy calculations. Moreover, the cubic phase has the lowest volume among the studied phases. In addition, $BaYO_3$ cubic phase do not transform to the other phases at positive pressures. From now on, only the results for the cubic phase will be given not to cover a lot of space in the journal.

Electronic properties

The band structure for $BaYO_3$ cubic phase has been calculated along the high symmetry points in the first Brillioun zone shown in Fig. 4. $BaYO_3$ cubic phase has a direct band gap which is 4.30 eV. Moreover, partial density of states obtained from the band structure is given in Fig. 5. The most significant

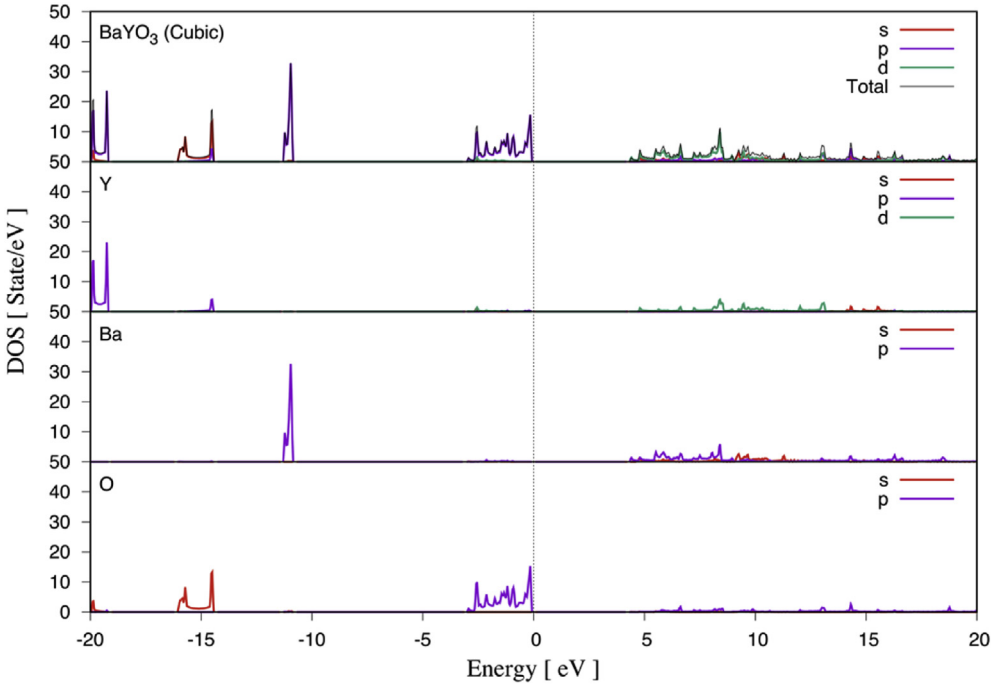

Fig. 5 – Partial density of states for $BaYO_3$ cubic phase.

contribution comes from Y and Ba atoms above the Fermi level for $BaYO_3$ cubic phase as can be concluded from Fig. 5.

$BaYO_3$ cubic phase has ionic bonding that can be seen from the charge density plot given in Fig. 6. In addition, Bader partial charge calculation has been performed using VASP and the analysis of the results has been done using the algorithm developed by Henkelman group. Table 2 lists the Bader partial net charge for each atom of $BaYO_3$ cubic phase. The total Bader net charge is zero. Also, the bond length between Y–O is 2.21 Å and it is 3.13 Å for Ba–O.

Mechanical properties

Elastic constants (C_{ij}) have been calculated in order to obtain mechanical properties of $BaYO_3$ cubic phase. C_{11}, C_{22} and C_{44} are required constants for a cubic phase and the calculated values for $BaYO_3$ cubic phase are given in Table 3. Moreover, the elastic constants for the other phases are given in Table 3 in order to contribute to the literature. The mechanical stability of a material could be determined with the Born stability criteria [42] and all phases of $BaYO_3$ except orthorhombic phase are mechanically stable. These calculated elastic constants have been used to obtain the mechanical properties.

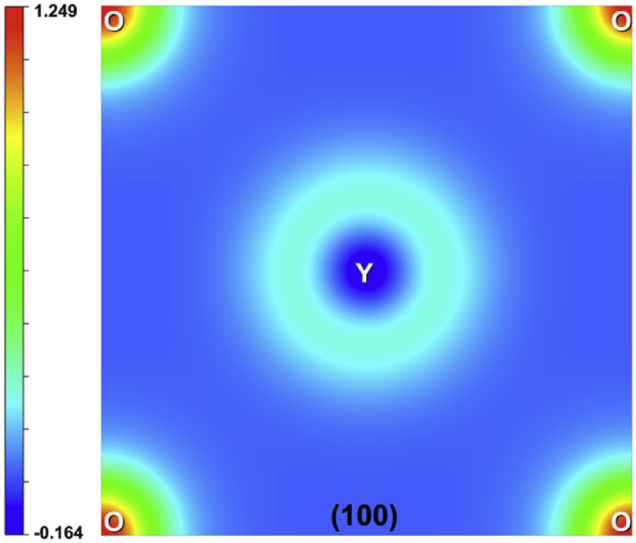

Fig. 6 – Charge density plot for $BaYO_3$ cubic phase.

Table 2 – Bader net charge for $BaYO_3$ cubic phase.

	Bader Net Charge
Ba	1.539
Y	1.995
O	−1.178

Table 4 – Bulk modulus (B in GPa), shear modulus (G in GPa), Young's modulus (E in GPa), Poisson's ratio, B/G ratio and hardness (H_v in GPa) for the five possible phases of $BaYO_3$.

	B	G	E	ν	B/G	H_v
Tetragonal (P4mm)	78.1	18.6	51.7	0.390	4.199	1.9
Rhombohedral (R-3c)	76.6	26.6	71.4	0.334	2.897	1.0
Hexagonal ($P6_3/mmc$)	70.8	23.4	63.2	0.351	3.025	0.4
Cubic (Pm-3m)	86.1	45.8	116.7	0.274	1.880	7.1

Bulk modulus, shear modulus, Young's modulus, Poisson's ratio, B/G ratio and hardness for $BaYO_3$ phases have been obtained using the calculated elastic constants and given in Table 4. Bulk modulus (B) is the measure of the incompressibility when a pressure applied. Shear modulus (G) is also called modulus of rigidity and it is known as the ratio of the shear stress to shear strain. Young's modulus (E) is also called elastic modulus and it is a measure of the elastic deformations. $BaYO_3$ cubic phase has the highest bulk modulus, shear modulus and Young's modulus. Poisson's ratio (ν) is used to determine the bonding nature of a material and defined as the transverse strain to axial strain ratio. The material that has ionic bonding, has ν value of 0.25 and if ν is around 0.1, the material has covalent bonding [43]. $BaYO_3$ cubic phase has ionic bonding as can be concluded from Table 4. B/G ratio is calculated to determine whether the material brittle or ductile. If B/G ratio is higher than 1.75, the material is ductile, vice versa for brittleness. $BaYO_3$ cubic phase is ductile. For the last parameter, hardness of a material could be calculated using Chen et al. approach [44]. The cubic phase of $BaYO_3$ is the hardest phase.

The directional dependent mechanical properties are important because they are used to determine material characteristics for plastic deformations, micro cracks, etc. Therefore, anisotropic elastic properties must be calculated. The calculated elastic constants have been employed to ELATE program [45]. Fig. 7 shows the directional dependent Young's modulus, linear compressibility, Shear modulus and Poisson's ratio in 3D and 2D for $BaYO_3$ cubic phase. The green curves or spheres show the maximum points for the parameter and the blue ones show the minimum. Also, if the spherical shape is distorted that means the anisotropy [46]. Young's modulus, shear modulus and Poisson's ratio are anisotropic in all planes while linear compressibility is

Table 3 – Elastic constants (C_{ij} in GPa) for the five possible phases of $BaYO_3$.

	C_{11}	C_{12}	C_{13}	C_{22}	C_{23}	C_{33}	C_{44}	C_{55}	C_{66}
Orthorhombic (Pnma)	82.9	69.8	69.2	55.6	74.7	55.3	−14.1	−1.2	−0.5
Tetragonal (P4mm)	135.5	46.7	52.7			128.1	34.0		1.6
Rhombohedral (R-3c)	132.2	67.7	50.3			100.9	21.1		30.2
Hexagonal ($P6_3/mmc$)	136.0	98.6	38.1			76.9	23.1		18.6
Cubic (Pm-3m)	182.6	37.9					33.5		

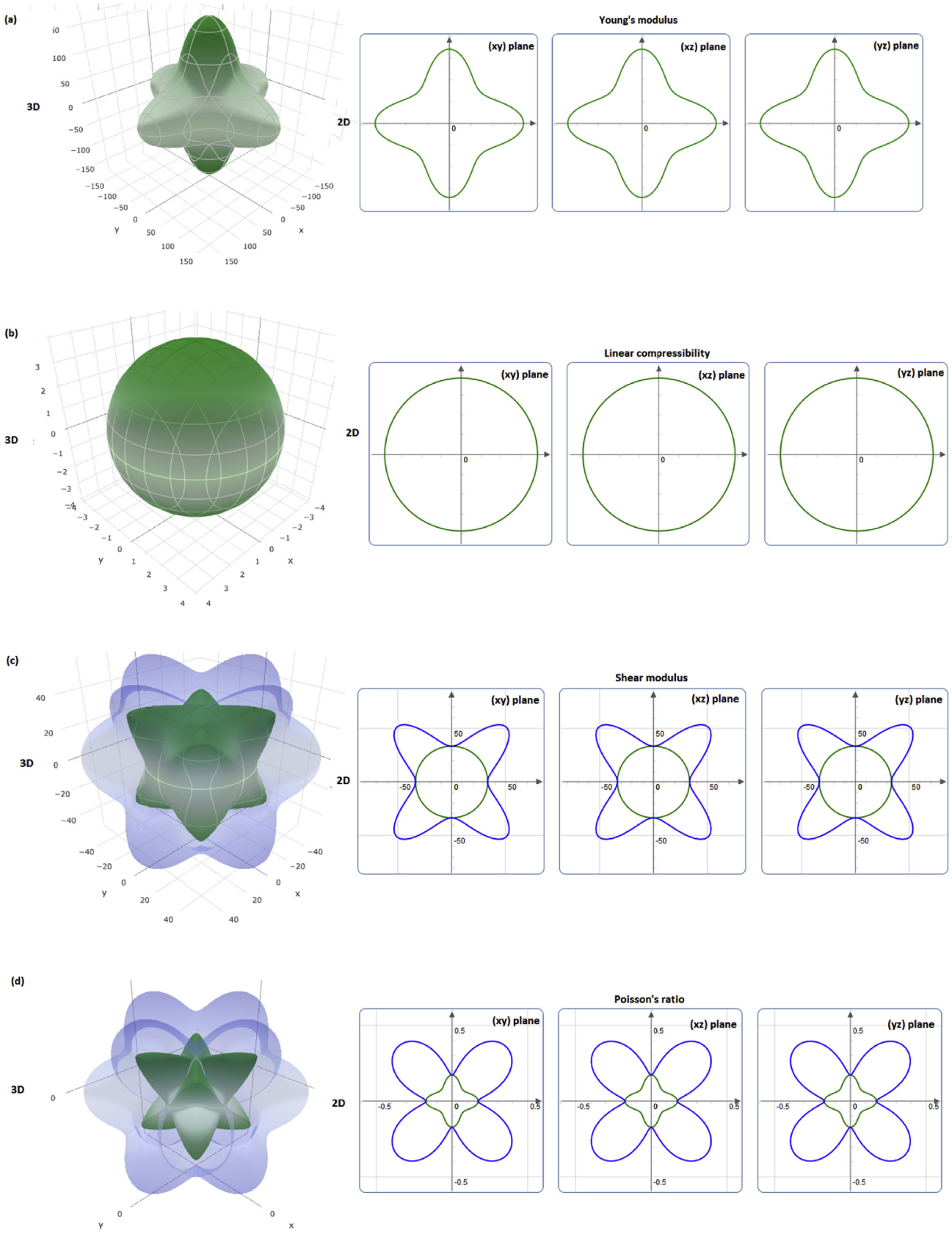

Fig. 7 – The direction dependent (a) Young's modulus, (b) linear compressibility, (c) shear modulus and (d) Poisson's ratio for the cubic phase of $BaYO_3$.

isotropic in all planes. Young's modulus has the highest values at the x, y and z axis, while shear modulus and Poisson's ratio have the highest values at 45° of xy, xz and yz planes.

Hydrogen bonding studies

The hydrogen bonding studies could be performed after obtaining main physical properties for the cubic phase of $BaYO_3$. The cubic phase is chosen for the hydrogen bonding studies because it is the most stable phase and it has the lowest volume among the other phases. The cubic phase of $BaYO_3$ belongs to 221 (Pm-3m) space group where Ba atoms are at the 1b site, Y atoms are at the 1a site and O atoms are at the 3d site Wyckoff positions.

Wyckoff position of 3c has been chosen for the hydrogen position where three hydrogen atoms have been added to the structure and $BaYO_3H_3$ chemical formula has been obtained. Fig. 8 shows the crystal structure of $BaYO_3H_3$.

After the structural optimization, the calculated lattice constant (a, in Å) is 4.55 and the calculated formation energy (ΔE_f) is −0.81 eV/atom that implies that $BaYO_3H_3$ is stable and synthesizable. The energy required to remove one hydrogen atom from $BaYO_3H_3$ must be calculated and it is defined as cohesive energy as can be calculated using Equation (2). The calculated cohesive energy is −1.10 eV/atom.

$$E_{cohesive} = \frac{\left(E_{BaYO_3H_3} - E_{BaYO_3}\right)}{3} \quad (2)$$

$BaYO_3H_3$ has been optimized and it has been found that $BaYO_3H_3$ is stable and synthesizable. Hydrogen storage materials should satisfy some criteria and gravimetric hydrogen storage capacity is one of them. The gravimetric hydrogen storage capacity is the amount of hydrogen stored per unit mass of a material [47]. The gravimetric storage capacity can be calculated using Equation (3) where H/M is the hydrogen to material atom ratio, M_H is the molar mass of hydrogen and M_{Host} is the molar mass of the material [47]. $BaYO_3H_3$ has 1.09 wt% gravimetric hydrogen storage capacity.

$$C_{wt\%} = \left(\frac{\left(\frac{H}{M}\right) M_H}{M_{Host} + \left(\frac{H}{M}\right) M_H} \times 100 \right) \% \quad (3)$$

After the study with $BaYO_3H_3$, six more hydrogen atoms bonded to $BaYO_3H_3$ at 6e Wyckoff positions and chemical formula of $BaYO_3H_9$ has been obtained. Fig. 9 shows the crystal structure of $BaYO_3H_9$. After the structural optimization, the calculated lattice constant (a, in Å) is 5.97 and the calculated formation energy (ΔE_f) is 0.35 eV. The positive formation energy implies that this structure is unstable and cannot be synthesized. Therefore, $BaYO_3H_9$ is not a good choice for hydrogen storage.

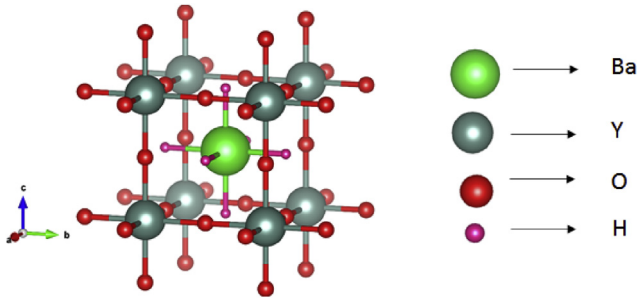

Fig. 8 – Crystal structure of $BaYO_3H_3$.

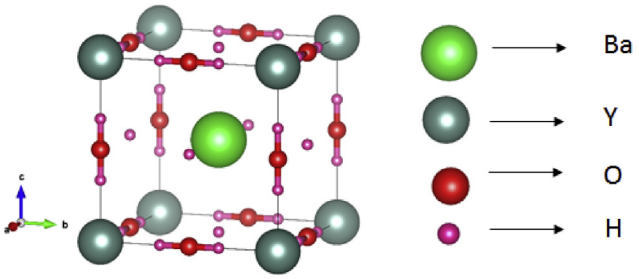

Fig. 9 – Crystal structure of $BaYO_3H_9$.

Conclusion

The structural, electronic and mechanical properties for $BaYO_3$ and $BaYO_3H_x$ perovskite have been calculated by first-principles calculation within the generalized gradient approximation based on density functional formalism. For this purpose, $BaYO_3$ has been investigated for five possible crystal structures and it has been found that the cubic phase is the most stable phase at positive pressures and has the lowest volume among the studied phases. After determining the most stable structure, mechanical and electronic properties have been investigated. The mechanical stability criteria have been satisfied for all these phases except the orthorhombic phase. $BaYO_3$ cubic phase has ionic bonding and it is a ductile material. Also, cubic phase is the hardest phase among the investigated phases. Moreover, direction dependent Young's modulus has the highest values at x, y and z axis, while shear modulus and Poisson's ratio have the highest values at 45° of xy, xz and yz planes. In addition, the band gap of $BaYO_3$ has been calculated as 4.30 eV which is a direct band gap. After these calculations, the hydrogen has been bonded and $BaYO_3H_3$ has been obtained. $BaYO_3H_3$ has a negative formation energy, therefore it is stable and synthesizable. In addition, the gravimetric hydrogen storage capacity has been calculated for $BaYO_3H_3$ which is 1.09 wt%. More hydrogen bonding studies have been performed, such as $BaYO_3H_9$ has been obtained but the structures are unstable and cannot be suitable for hydrogen storage purposes. This study is a first attempt to consider the perovskite materials for solid state hydrogen storage method as authors know up to date and could be useful for future theoretical and experimental studies for the perovskite materials and hydrogen storage.

Acknowledgments

This work was supported by the Ahi Evran University Research Project Unit under Project No PYO-KMY.4001.15.001.

REFERENCES

[1] Züttel A. Hydrogen storage methods. Naturwissenschaften 2004;91:157–72. https://doi.org/10.1007/s00114-004-0516-x.

[2] Eberle U, Felderhoff M, Schüth F. Chemical and physical solutions for hydrogen storage. Angew Chem Int Ed 2009;48:6608–30. https://doi.org/10.1002/anie.200806293.

[3] Walker G(Gavin). Institute of materials M. solid state hydrogen storage : materials and chemistry. Woodhead Pub.; 2008.

[4] van den Berg AWC, Areán CO. Materials for hydrogen storage: current research trends and perspectives. Chem Commun 2008;0:668–81. https://doi.org/10.1039/B712576N.

[5] Jain IP, Jain P, Jain A. Novel hydrogen storage materials: a review of lightweight complex hydrides. J Alloy Comp 2010;503:303–39. https://doi.org/10.1016/J.JALLCOM.2010.04.250.

[6] Broom DP. Hydrogen sorption properties of materials. 2011. p. 61–115. https://doi.org/10.1007/978-0-85729-221-6_3.

[7] Züttel A, Wenger P, Rentsch S, Sudan P, Mauron P, Emmenegger C. $LiBH_4$ a new hydrogen storage material. J Power Sources 2003;118:1–7. https://doi.org/10.1016/S0378-7753(03)00054-5.

[8] Chen P, Xiong Z, Luo J, Lin J, Lee Tan K. Interaction of hydrogen with metal nitrides and imides. Nature 2002;420:302–4. https://doi.org/10.1038/nature01210.

[9] Bogdanović B, Schwickardi M. Ti-Doped $NaAlH_4$ as a hydrogen -storage material-prerparation by Ti-catalyzed hydrogenation of aluminium powder in conjuction with sodium hydride. Appl Phys Mater Sci Process 2001;72:221–3. https://doi.org/10.1007/s003390100774.

[10] Imamura H, Masanari K, Kusuhara M, Katsumoto H, Sumi T, Sakata Y. High hydrogen storage capacity of nanosized magnesium synthesized by high energy ball-milling. J Alloy Comp 2005;386:211–6. https://doi.org/10.1016/j.jallcom.2004.04.145.

[11] Zaluska A, Zaluski L, Ström-Olsen JO. Nanocrystalline magnesium for hydrogen storage. J Alloy Comp 1999;288:217–25. https://doi.org/10.1016/S0925-8388(99)00073-0.

[12] Lee SM, Lee YH, Hee Y. Hydrogen storage in single-walled carbon nanotubes Hydrogen storage in single-walled carbon nanotubes 2011;2877:13–6. https://doi.org/10.1063/1.126503.

[13] Rosi NL, Eckert J, Eddaoudi M, Vodak T, Kim J, Keeffe MO, et al. Hydrogen storage in microporous metal-organic frameworks. Science 2003;300:1127–30.

[14] Chen P. High H_2 uptake by alkali-doped carbon nanotubes under ambient pressure and moderate temperatures. Science 1999;285(80):91–3. https://doi.org/10.1126/science.285.5424.91.

[15] Dillon AC, Jones KM, Bekkedahl TA, Kiang CH, Bethune DS, Heben MJ. Storage of hydrogen in single-walled carbon nanotubes. Nature 1997;386:377–9. https://doi.org/10.1038/386377a0.

[16] Floriano R, Deledda S, Hauback BC, Leiva DR, Botta WJ. Iron and niobium based additives in magnesium hydride: microstructure and hydrogen storage properties. Int J Hydrogen Energy 2017;42:6810–9. https://doi.org/10.1016/J.IJHYDENE.2016.11.117.

[17] Sadhasivam T, Kim H-T, Jung S, Roh S-H, Park J-H, Jung H-Y. Dimensional effects of nanostructured Mg/MgH_2 for hydrogen storage applications: a review. Renew Sustain Energy Rev 2017;72:523–34. https://doi.org/10.1016/J.RSER.2017.01.107.

[18] Jain IP, Lal C, Jain A. Hydrogen storage in Mg: a most promising material. Int J Hydrogen Energy 2010;35:5133–44. https://doi.org/10.1016/J.IJHYDENE.2009.08.088.

[19] Hanada N, Ichikawa T, Orimo S-I, Fujii H. Correlation between hydrogen storage properties and structural characteristics in mechanically milled magnesium hydride MgH_2. J Alloy Comp 2004;366:269–73. https://doi.org/10.1016/S0925-8388(03)00734-5.

[20] Ćirić KD, Koteski VJ, Stojić DL j, Radakovic JS, Ivanovski VN. HfNi and its hydrides – first principles calculations. Int J Hydrogen Energy 2010;35:3572–7. https://doi.org/10.1016/J.IJHYDENE.2010.01.127.

[21] Chattaraj D, Dash S, Majumder C. Structural, electronic, elastic, vibrational and thermodynamic properties of ZrNi and $ZrNiH_3$: a comprehensive study through first principles approach. Int J Hydrogen Energy 2016;41:20250–60. https://doi.org/10.1016/J.IJHYDENE.2016.09.046.

[22] Baysal MB, Surucu G, Deligoz E, Ozısık H. The effect of hydrogen on the electronic, mechanical and phonon properties of $LaMgNi_4$ and its hydrides for hydrogen storage applications. Int J Hydrogen Energy 2018;43:23397–408. https://doi.org/10.1016/J.IJHYDENE.2018.10.183.

[23] Bogdanović B, Schwickardi M. Ti-doped alkali metal aluminium hydrides as potential novel reversible hydrogen storage materials. J Alloy Comp 1997:253–4. https://doi.org/10.1016/S0925-8388(96)03049-6. 1–9.

[24] Martínez-Coronado R, Sánchez-Benítez J, Retuerto M, Fernández-Díaz MT, Alonso JA. High-pressure synthesis of $Na_{1-x}Li_xMgH_3$ perovskite hydrides. J Alloy Comp 2012;522:101–5. https://doi.org/10.1016/J.JALLCOM.2012.01.097.

[25] Ikeda K, Kogure Y, Nakamori Y, Orimo S. Formation region and hydrogen storage abilities of perovskite-type hydrides. Prog Solid State Chem 2007;35:329–37. https://doi.org/10.1016/J.PROGSOLIDSTCHEM.2007.01.005.

[26] Bouhadda Y, Fenineche N, Boudouma Y. Hydrogen storage: lattice dynamics of orthorhombic $NaMgH_3$. Phys B Condens Matter 2011;406:1000–3. https://doi.org/10.1016/J.PHYSB.2010.12.048.

[27] Rehmat B, Rafiq MA, Javed Y, Irshad Z, Ahmed N, Mirza SM. Elastic properties of perovskite-type hydrides $LiBeH_3$ and $NaBeH_3$ for hydrogen storage. Int J Hydrogen Energy 2017;42:10038–46. https://doi.org/10.1016/J.IJHYDENE.2017.01.109.

[28] Gencer A, Surucu G. Investigation of structural, electronic and lattice dynamical properties of $XNiH_3$ (X = Li, Na and K) perovskite type hydrides and their hydrogen storage applications. Int J Hydrogen Energy 2019;44:15173–82. https://doi.org/10.1016/J.IJHYDENE.2019.04.097.

[29] Ikeda K, Kogure Y, Nakamori Y, Orimo S. Reversible hydriding and dehydriding reactions of perovskite-type hydride $NaMgH_3$. Scripta Mater 2005;53:319–22. https://doi.org/10.1016/J.SCRIPTAMAT.2005.04.010.

[30] Li Y, Mi Y, Chung JS, Kang SG. First-principles studies of $K_{1-x}M_xMgH_3$ (M = Li, Na, Rb, or Cs) perovskite hydrides for hydrogen storage. Int J Hydrogen Energy 2018;43:2232–6. https://doi.org/10.1016/J.IJHYDENE.2017.10.175.

[31] Wang Z, Tao S, Deng J, Zhou H, Yao Q. Significant improvement in the dehydriding properties of perovskite hydrides, $NaMgH_3$, by doping with K_2TiF_6. Int J Hydrogen Energy 2017;42:8554–9. https://doi.org/10.1016/J.IJHYDENE.2016.12.078.

[32] Gencer A, Surucu G, Al S. $MgTiO_3H_x$ and $CaTiO_3H_x$ perovskite compounds for hydrogen storage applications. Int J Hydrogen Energy 2019;44:11930–8. https://doi.org/10.1016/J.IJHYDENE.2019.03.116.

[33] Kresse G, Furthmüller J. Efficiency of ab-initio total energy calculations for metals and semiconductors using a plane-wave basis set. Comput Mater Sci 1996;6:15–50. https://doi.org/10.1016/0927-0256(96)00008-0.

[34] Kresse G, Furthmüller J. Efficient iterative schemes for *ab initio* total-energy calculations using a plane-wave basis set.

Phys Rev B 1996;54:11169–86. https://doi.org/10.1103/PhysRevB.54.11169.
[35] Perdew JP, Burke K, Ernzerhof M. Generalized gradient approximation made simple. Phys Rev Lett 1996;77:3865–8. https://doi.org/10.1103/PhysRevLett.77.3865.
[36] Blöchl PE. Projector augmented-wave method. Phys Rev B 1994;50:17953–79. https://doi.org/10.1103/PhysRevB.50.17953.
[37] Kresse G, Joubert D. From ultrasoft pseudopotentials to the projector augmented-wave method. Phys Rev B 1999;59:1758–75. https://doi.org/10.1103/PhysRevB.59.1758.
[38] Pack JD, Monkhorst HJ. Special points for Brillouin-zone integrations—a reply. Phys Rev B 1977;16:1748–9. https://doi.org/10.1103/PhysRevB.16.1748.
[39] Monkhorst HJ, Pack JD. Special points for Brillouin-zone integrations. Phys Rev B 1976;13:5188–92. https://doi.org/10.1103/PhysRevB.13.5188.
[40] Bader RFW. Atoms in molecules : a quantum theory. Clarendon Press; 1990.
[41] Erkişi A, Gökoğlu G, Sürücü G, Ellialtıoğlu R, Yıldırım EK. First-principles investigation of $LaGaO_3$ and $LaInO_3$ lanthanum perovskite oxides. Philos Mag A 2016;96:2040–58. https://doi.org/10.1080/14786435.2016.1189100.
[42] Born M, Misra RD. On the stability of crystal lattices. IV. Math Proc Camb Philos Soc 1940;36:466. https://doi.org/10.1017/S0305004100017515.
[43] Bannikov VV, Shein IR, Ivanovskii AL. Electronic structure, chemical bonding and elastic properties of the first thorium-containing nitride perovskite $TaThN_3$. Phys Status Solidi Rapid Res Lett 2007;1:89–91. https://doi.org/10.1002/pssr.200600116.
[44] Chen X-Q, Niu H, Li D, Li Y. Modeling hardness of polycrystalline materials and bulk metallic glasses. Intermetallics 2011;19:1275–81. https://doi.org/10.1016/J.INTERMET.2011.03.026.
[45] Gaillac R, Pullumbi P, Coudert F-X. ELATE: an open-source online application for analysis and visualization of elastic tensors. J Phys Condens Matter 2016;28. https://doi.org/10.1088/0953-8984/28/27/275201. 275201.
[46] Surucu G. Investigation of structural, electronic, anisotropic elastic, and lattice dynamical properties of MAX phases borides: an Ab-initio study on hypothetical M_2AB (M = Ti, Zr, Hf; A = Al, Ga, In) compounds. Mater Chem Phys 2018;203:106–17. https://doi.org/10.1016/J.MATCHEMPHYS.2017.09.050.
[47] Broom DP. Hydrogen sorption properties of materials. 2011. p. 61–115. https://doi.org/10.1007/978-0-85729-221-6_3.